Entropy-Controlled 2D Supramolecular Structures of *N,N′*-Bis(*n*-alkyl)-naphthalenediimides on a HOPG Surface

Yusuke Miyake,[†] Toshi Nagata,[†,*] Hirofumi Tanaka,[†,‡] Masashi Yamazaki,[§] Masahiro Ohta,[§] Ryohei Kokawa,[§] and Takuji Ogawa[†,‡,*]

[†]Research Center for Molecular-Scale Nanoscience, Institute for Molecular Science, 5-1 Higashiyama, Myodaiji, Okazaki 444-8787, Japan, [‡]Department of Chemistry, Graduate School of Science, Osaka University, 1-1 Matikaneyama-cho, Toyonaka, Osaka 560-0043, Japan, and [§]Surface Analysis Business Unit, Analytical & Measuring Instrument Division, Shimadzu Corporation, 1 Nishinokyo-Kuwabaracho, Nakagyo-ku, Kyoto 604-8511, Japan

ABSTRACT

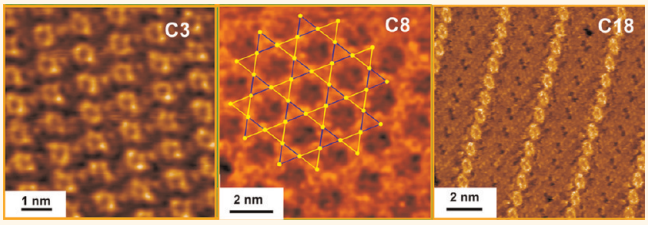

The two-dimensional supramolecular structures of a series of *N,N′*-bis(*n*-alkyl)-naphthalenediimides (NDIs), whose chain lengths span from C3 to C18, at a liquid−HOPG surface interface, studied by STM and FM-AFM, are assigned with the help of molecular dynamics/molecular mechanics calculations to demonstrate that the C3- and C4-NDIs show lamellar structures, the C4- to C12-NDIs show honeycomb (KAGOME) structures, and the C14- to C18-NDIs show lamellar structures again. The change in supramolecular structure depending on chain length can be explained semiquantitatively by the balance of entropy and enthalpy terms to show the importance of "self-avoiding walk" of the alkyl chain in entropy terms.

KEYWORDS: supramolecular structure · naphthalenediimide · HOPG surface · STM · FM-AFM · molecular dynamics · entropy · self-avoiding walk

Supramolecular two-dimensional structures on surfaces have attracted much attention for purely academic reasons as well as for their use in designing electronic and optoelectronic devices at the molecular scale.[1−5] It is difficult to design or predict the supramolecular structure from the unit molecular structure because the supramolecular structure is determined by various parameters, such as molecule−molecule, molecule−substrate, and molecule−solvent interactions.[6−16] Although there has been a significant effort to analyze these parameters in order to realize "two-dimensional crystal engineering",[17] it remains as a challenging task.

In this work, we systematically analyzed the supramolecular structures of a series of *N,N′*-bis(*n*-alkyl)naphthalenediimides whose alkyl chain lengths span from C3 to C18 (abbreviated as **C3-NDI** *etc.*; structures are shown in Figure 1) at the liquid−solid interface on highly oriented pyrolytic graphite (HOPG) by scanning tunneling microscopy (STM), frequency-modulation atomic force microscopy (FM-AFM), molecular dynamics (MD), and molecular mechanics (MM) calculations. We will discuss the importance of the entropy term to account for the versatility of the supramolecular structures that depend on the chain lengths of the molecules.

RESULTS AND DISCUSSION

Supramolecular Images of *N,N′*-Bis(*N*-alkyl)-naphthalenediimides (C*x*-NDIs, *x* = 3−18) on HOPG, Observed by STM. The images of the supramolecular structures of **C*x*-NDIs** on HOPG, measured by STM, are shown in Figure 2, and the observed unit cell parameters are tabulated in Table 1.

The image of **C3-NDI** shows lamellar structures (Figure 2a, in which the fine structure of the naphthalene π electronic system can be seen as an annular shape. **C4-NDI** shows three types of images: lamellar (Figure 2c), zigzag (Figure 2d), and honeycomb structures (Figure 2e). The lamellar structure was the dominant image; however, it contained several defects when compared with **C3-NDI**. **C5-NDI** shows only the honeycomb structure (Figure 2f). The **C6-** to **C9-NDIs** show a different type of honeycomb structure (Figure 2g−j). In order to distinguish it from the honeycomb images observed for the **C4-** and **C5-NDIs**, the former is labeled honeycomb B and the latter is labeled honeycomb A. The honeycomb A structure is characterized by chirality, whereas

* Address correspondence to ogawa@chem.sci.osaka-u.ac.jp, toshi-n@ims.ac.jp.

Received for review December 21, 2011 and accepted April 2, 2012.

Published online April 02, 2012
10.1021/nn205006d

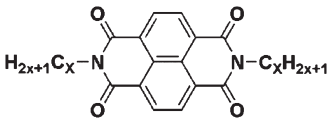

Figure 1. Structure of *N*,*N*′-bis(*N*-alkyl)naphthalenediimides (C*x*-NDIs, $x = 3-18$).

the honeycomb B structure is not chiral. Both of the two possible chirality images were observed for the **C4-** and **C5-NDIs**.

One important finding in the case of honeycomb B is that the areas per molecule calculated from the observed unit cell parameters are almost constant for these molecules; they are 1.17, 1.11, 1.19, and 1.1 nm^2 for **C6-**, **C7-**, **C8-**, and **C9-NDI**, respectively (Table 1 and Figure 3). The fact that the area per molecule is independent of the chain length strongly suggests that the alkyl chains stand up from the substrate surface and do not contribute to the two-dimensional supramolecular structures on the surface.

The **C10-** and **C12-NDIs** show a unique honeycomb shape, which was labeled honeycomb C (Figure 2l,n). The structural difference between honeycomb C and honeycomb A is that in honeycomb C the large holes are surrounded by a dark Y shape and that other smaller holes are present between the large holes. **C11-NDI** exhibited a hexagonal shape similar to honeycomb B, with superlattice stripes; it was labeled honeycomb D (Figure 2m).

The **C13-** to **C18-NDIs** show lamellar images; however, the alignment parameters to the HOPG substrate were different from those in **C3-NDI** (Figure 4). In order to distinguish between these two lamellar images on the basis of the type of lamellae that can be seen in them, supramolecular structures of the **C3**- and **C4-NDIs** are labeled lamella A and those of the **C13-** to **C18-NDIs** are labeled lamella B. The differences in the alignment parameters are described in the caption to Figure 4.

Frequency-Modulated Atomic Force Microscopy (FM-AFM) of the C3-, C9-, and C18-NDIs at the HOPG–Water Interface. Although STM measurements afford the best spatial resolution of molecular assemblies of the various scanning probe microscopic (SPM) methods, their images do not correspond to the actual molecular shape. Since STM measures the tunneling current through the molecules, π-bonds with higher energy orbitals appear brighter than σ-bonds. Further, the long alkyl chains standing up from the substrate surface cannot be observed by STM because of the low tunneling current that flows through them. In contrast, AFM gives the images of molecular shapes more directly since it measures the interaction force between the cantilever and the molecules. However, the usual AFM measurements in the tapping mode or contact mode do not afford molecular scale resolution because they measure the repulsive force between the many atoms of the cantilever and those of the target molecules. In order to obtain molecular or atomic level resolution, we need to reduce the number of interacting atoms by increasing the distance between the cantilever and the molecules. This method is often called the *noncontact mode*, and it is usually performed under high vacuum conditions to increase the *Q* value of the cantilever and to avoid the contamination of the substrate surface. It is argued that water molecules may act as a lubricant layer when the method is carried out under liquid conditions, thus enabling true atomic resolution imaging. Although the influence of the tip size and the forces acting on the surface remain even under these conditions, atomic resolution can be realized by the precise control of the tip–sample interaction by using frequency-modulation AFM (FM-AFM).[18–20]

First, the measurements were attempted in the same solvent (1-tetradecene) as that used for the STM measurements; however, for unknown reasons, no good images were obtained. By changing the solvent to ultrapure water, images at molecular level resolution were successfully obtained. FM-AFM images of **C3-NDI**, **C9-NDI**, and **C18-NDI** are shown in Figure 2b,k,t, respectively. For **C3-NDI** and **C18-NDI**, almost the same structures as those in the STM were observed, with slight differences in the cell parameters. For **C9-NDI**, the cell parameters were similar to those observed by STM; however, the apparent image was different. For easy understanding of the image comparison of AFM and STM of **C9-NDI**, eye guidance is shown in Figure S7 in the Supporting Information.

Model Structures by Molecular Mechanics Calculations. For the lamellar structures observed in the **C3-**, **C4-**, and **C13-** to **C18-NDIs**, the supramolecular structures can be assigned without difficulty. However, assignment of the supramolecular structures of other honeycomb images obtained by STM or FM-AFM requires further considerations. Discussions on the assignment of supramolecular structures of similar systems are still being conducted, as described by the following text.

An STM investigation of the two-dimensional supramolecular structures of similar molecules, *N*,*N*′-dialkylperylenediimides (PTCDI, alkyl is *n*-C_4, C_8, C_{12}, C_{13}, C_{18}), at the interface of liquid and HOPG or MoS_2 surfaces is reported.[21] On the HOPG surface, **C4-**, **C8-**, **C12-**, and **C13-PTCDIs** show rectangular STM images, which can be assigned to the so-called "herringbone" structures, where every other row of molecules has the same molecular orientation. The proposed supramolecular structure is almost the same as that observed for perylenetetracarboxylic dianhydride (PTCDA), whose high-resolution STM images on HOPG are available.[22] For **C18-PTCDI**, both the rectangular structure and the row structure are observed; the latter is the same as the lamellar structure mentioned here. As the molecular area of the rectangular polytype remains approximately constant, the authors suggest that the alkyl tails of the PTCDI cores protrude above the

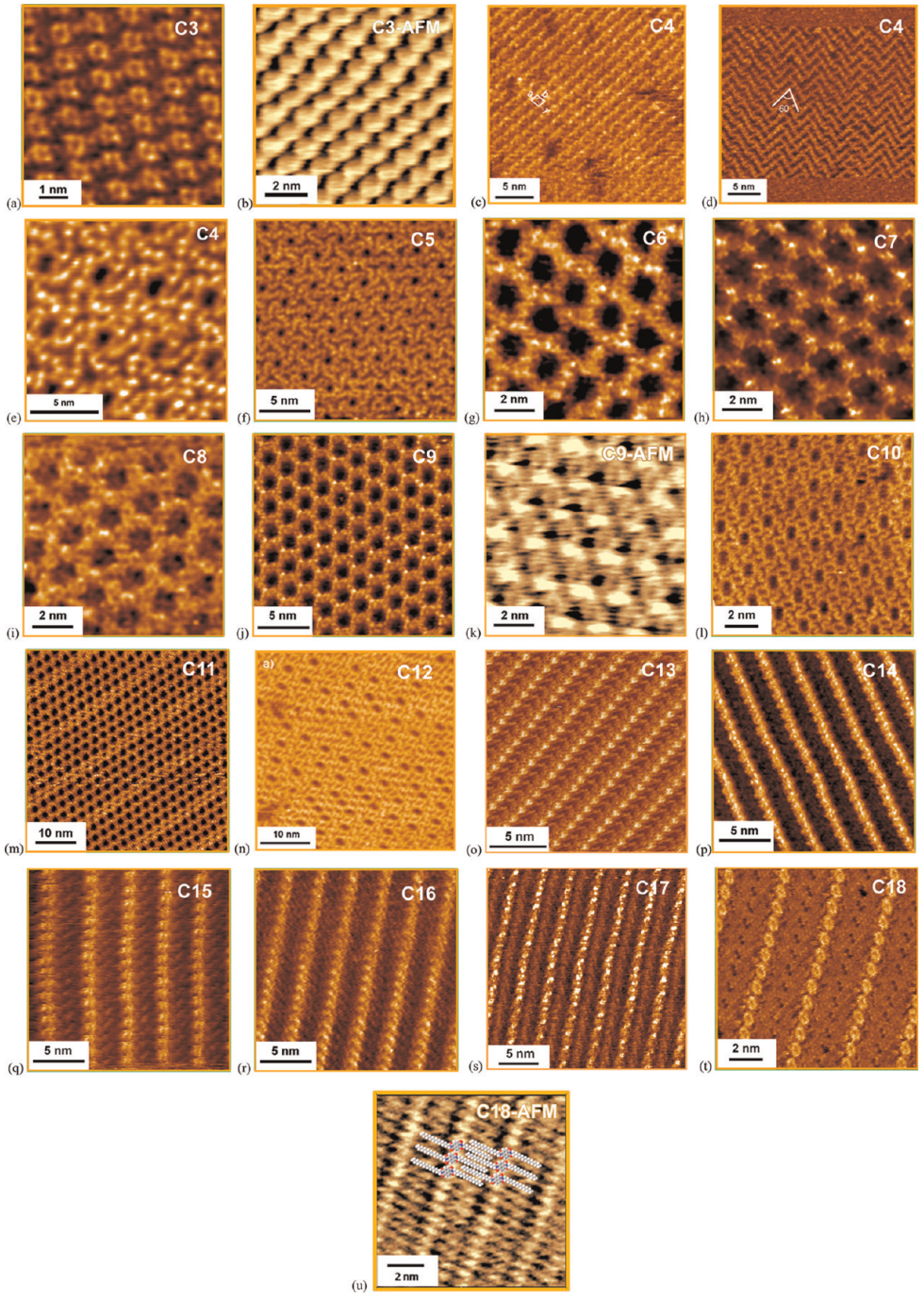

Figure 2. STM and FM-AFM images of the C*x*-NDIs at the interface of the 1-tetradecene solution (for STM) (~5.0×10^{-4} M) or water (for FM-AFM) and graphite. Details for the preparation method of the samples are described in the Methods. (a) STM image of C3-NDI (lamella A structure). Scanning area is 7.06×7.06 nm^2 $I = 59$ pA and V_s (bias voltage) = −1.200 V. (b) FM-AFM image of C3-NDI at the interface of water and graphite. (c) STM image of C4-NDI (lamella A structure). Scanning area is 20 × 20 nm^2; $I = 10$ pA and $V_s = 1.600$ V. (d) STM image of C4-NDI (zigzag structure). Scanning area is 29.8×29.8 nm^2; $I = 9$ pA and $V_s = 1.600$ V. (e) STM image of C4-NDI (honeycomb A structure). Scanning area is 15.0×15.0 nm^2; $I = 9$ pA and $V_s = 1.600$ V. (f) STM image of C5-NDI (honeycomb A structure). Scanning area is 29.9×29.9 nm^2; $I = 9$ pA and $V_s = 1.600$ V. (g) STM image of C6-NDI. Scanning area is 10.1×10.1 nm^2; $I = 84$ pA and $V_s = 1.550$ V. (h) STM image of C7-NDI. Scanning area is 10.1×10.1 nm^2; $I = 20$ pA and $V_s = 1.370$ V. (i) STM image of C8-NDI (honeycomb B). Scanning area is 10.1×10.1 nm^2; $I = 11$ pA and $V_s = 1.572$ V. (j) STM image of C9-NDI. Scanning area is 19.7×19.7 nm^2; $I = 71$ pA and $V_s = 1.498$ V. (k) FM-AFM image of C9-NDI. (l) STM image of C10-NDI (honeycomb C structure). Scanning area is 29.8×29.8 nm^2; $I = 11$ pA and $V_s = 1.540$ V. (m) STM image of C11-NDI. Scanning area is 49.7×49.7 nm^2; $I = 10$ pA and $V_s = 1.580$ V. (n) STM image of C12-NDI. Scanning area is 39.7×39.7 nm^2; $I = 9$ pA and $V_s = 1.600$ V. (o) STM image of C13-NDI. Scanning area is 17.7×17.7 nm^2; $I = 20$ pA and $V_s = -0.100$ V. (p) STM image of C14-NDI. Scanning area is 19.7×19.7 nm^2; $I = 9$ pA and $V_s = 1.200$ V. (q) STM image of C15-NDI. Scanning area is 19.8×19.8 nm^2; $I = 100$ pA and $V_s = -1.509$ V. (r) STM image of C16-NDI. Scanning area is 19.8×19.8 nm^2; $I = 38$ pA and $V_s = -1.129$ V. (s) STM image of C17-NDI. Scanning area is 25.0×25.0 nm^2; $I = 20$ pA and $V_s = -1.100$ V. (t) STM image of C18-NDI. Scanning area is 12.0×12.0 nm^2; $I = 98$ pA and $V_s = -1.069$ V. (u) FM-AFM image of C18-NDI. The assigned supramolecular structure for the image is shown with molecular modeling.

TABLE 1. Supramolecular Structures and Unit Cell Parameters of C*x*-NDIs on Graphite

		observed unit cell parameter by STM/molecular mechanics simulation					
imide	**supramolecular structure**	***a*/nm**	***b*/nm**	**γ/deg**	**A/nm^2**	**number of molecules in a cell**	**area per molecule/nm^2**
C3-NDI	lamella A	1.07 ± 0.04	1.38 ± 0.06	96	1.47	1	1.47
		0.92	*1.37*	*98.3*	*1.24*		
C4-NDI	lamella A	1.2 ± 0.2	1.7 ± 0.4	90	2.0	1	2.0
C4-NDI	honeycomb A	4.32 ± 0.04	4.43 ± 0.04	124	15.8	12	1.31
		4.28	*4.35*	*119.4*	*16.2*		
C5-NDI	honeycomb A	4.34 ± 0.04	4.41 ± 0.02	124	15.9	12	1.33
C6-NDI	honeycomb B	2.01 ± 0.03	2.01 ± 0.03	120	3.50	3	1.17
		2.00	*2.01*	*119.6*	*3.50*		
C7-NDI	honeycomb B	1.99 ± 0.05	2.13 ± 0.05	128	3.34	3	1.11
C8-NDI	honeycomb B	1.99 ± 0.05	2.06 ± 0.06	119	3.59	3	1.19
C9-NDI	honeycomb B	1.87 ± 0.09	2.1 ± 0.1	119	3.4	3	1.1
C10-NDI	honeycomb C	3.6 ± 0.2	5.2 ± 0.1	142	12	12	1.0
C11-NDI[a]	honeycomb D	2.4 ± 0.2	2.6 ± 0.1	116	5.6	3	1.9
C12-NDI	honeycomb C					*b*	
C13-NDI	lamella B	1.07 ± 0.05	2.9 ± 0.2	98	3.1	1	3.1
C14-NDI	lamella B	1.01 ± 0.07	3.02 ± 0.09	104	3.22	1	3.22
C15-NDI	lamella B	1.07 ± 0.06	3.1 ± 0.1	95	3.3	1	3.3
C16-NDI	lamella B	1.03 ± 0.09	3.4 ± 0.1	96	3.4	1	3.4
C17-NDI	lamella B	1.04 ± 0.03	3.3 ± 0.2	105	3.3	1	3.3
C18-NDI	lamella B	1.05 ± 0.03	3.5 ± 0.2	103	3.6	1	3.6
		0.90	*3.51*	*95.5*	*3.14*		
		0.91	*3.31*	*99.2*	*2.97*		

[a]The lattice constant of the supramolecular structure of **C11-NDI** is calculated from the region without superlattice structure. [b]Because of the frequent presence of superlattice in the structure, the unit cell parameters could not be determined precisely.

adsorbate layer into the solvent. However, because of the unstable supramolecular structures of the system, any further discussions on the assignment of the detailed supramolecular structures are likely to remain inconclusive.

Higher resolution STM images reported for *N*,*N*′-dioctylnaphthalenediimide (**C8-NDI**) on HOPG under ultrahigh vacuum conditions show a honeycomb structure, which is identical with that observed in this work.[23] The proposed supramolecular structure is an interdigitated lamellar structure with the alkane arms approximately flat on the surface. However, with this supramolecular structure, the constant molecular area observed for the **C6-** to **C10-NDIs** cannot be accounted for because, if the alkyl arms lie on the surface, the molecular area should be larger for longer arms. Therefore, to obtain reasonable supramolecular structures for the honeycomb images, molecular dynamics and molecular mechanics simulations were used.

Lamellar Structure. A geometry search of **C3-NDI** under periodic boundary conditions with $Z = 1$ (Z is the number of molecules contained in a unit cell) in an oblique unit cell gave a single, unique solution, as shown in Figure 5a. The NDI planes are parallel to the graphite surface, and neighboring molecules along the *b* axis interact with double hydrogen bonds, as observed in the X-ray structure of **C4-NDI**.[24]

Figure 5a also shows that the **C3-NDI** molecules are nearly close-packed in this structure. Therefore, the unit cell area of this structure (observed 1.47 nm^2, calculated 1.24 nm^2) provides a good estimation of the space that a single **C3-NDI** molecule occupies on the graphite surface. Even for **C*x*-NDI** molecules with longer alkyl chains ($x \geq 4$), it still provides an estimation of the *minimum* required area for one **C*x*-NDI** molecule to be accommodated. Later, we will use this value (1.24 nm^2) to calculate the *maximum* number of **C*x*-NDI** molecules that can be accommodated within the observed unit cell.

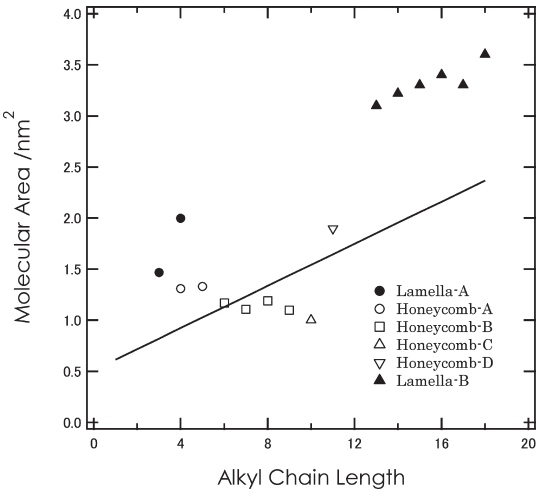

Figure 3. Plot of the area occupied by a single C*x*-NDI molecule on the graphite surface, as measured by STM, *vs* alkyl chain length. The line indicates the calculated area from the Connolly solvent excluded volume *vs* alkyl chain length.

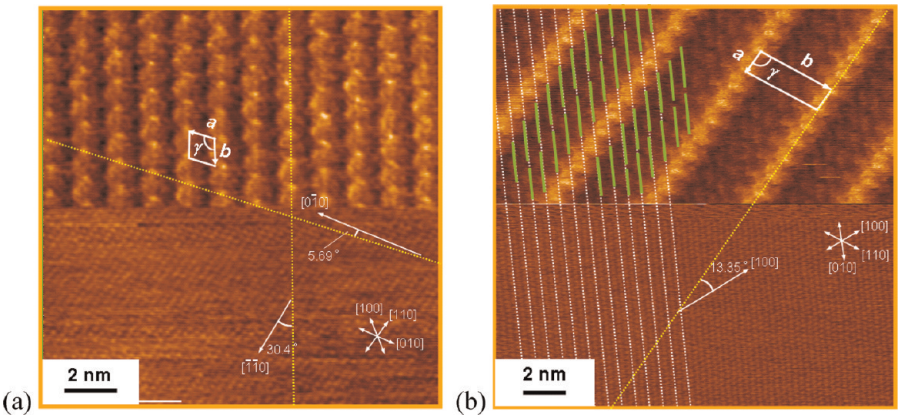

Figure 4. Lattice alignments of the C3-NDI and the C18-NDI with the substrate HOPG. (a) C3-NDI. Scanning area is 14.9 × 14.9 nm^2; I = 9 pA and V_s = −1.100 V for the upper part, and I = 9 pA and V_s = −0.05 V for the lower part. The upper part represents the STM image of C3-NDI; the lower part shows the graphite substrate underneath the molecules. Yellow dotted lines are the directions of C3-NDI lattice vectors. White arrows indicate the lattice directions of the graphite. The angle between molecular lattice vector a and [010] of the HOPG is 5.69°, and that between b and [110] is 30.4°. The molecular lattice vector b corresponds to the row of the naphthalene cores. (b) C18-NDI. Scanning area is 14.8 × 14.8 nm^2; I = 20 pA and V_s = −1.500 V for the top; I = 80 pA and V_s = −0.08 V for the bottom. The upper part of the image is the STM image of C18-NDI; the lower part is the graphite substrate. The white dotted lines located in the left part of the image represent the direction of the [010] vector of the graphite lattice. The thick green lines in the STM image represent the alkyl groups of the molecules. The white arrows in the right side of the lower part of the STM image represent the lattice direction of the graphite. In this image, the row of the naphthalene cores corresponds to molecular lattice vector a. The angle this vector of C18-NDI makes with [110] of the HOPG is 73.35°, which is about twice as large as that in C3-NDI. In another analysis, the alkyl groups of C18-NDI are almost coincident with the [010] lattice of the HOPG, while the alkyl groups of C3-NDI make an angle of 5.69° with the [010] lattice of the HOPG.

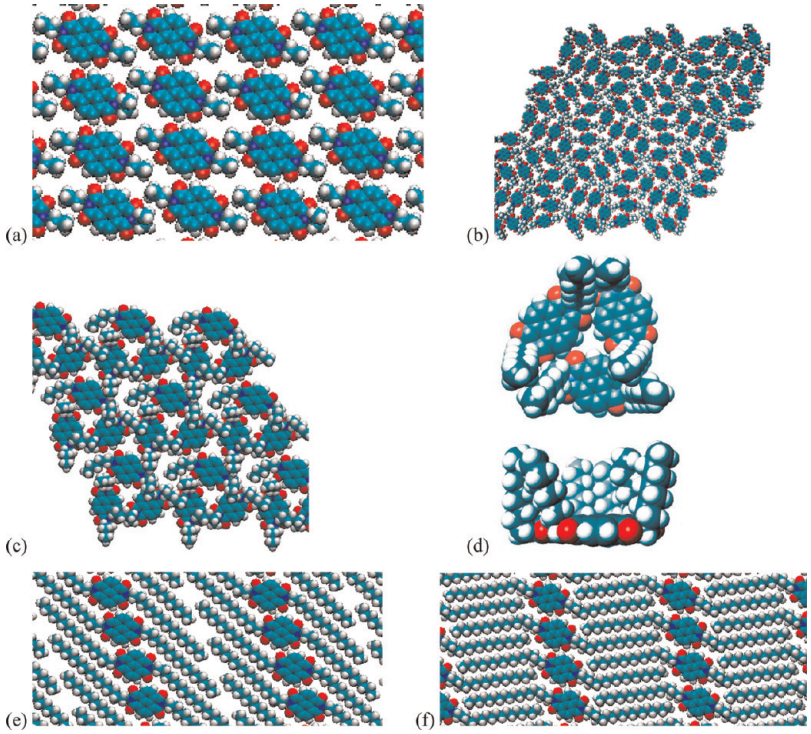

Figure 5. (a) Molecular modeling structure of C3-NDI on graphite, obtained by molecular dynamics (MD) and molecular mechanics (MM) calculations. The calculated unit cell parameters are a = 0.92 nm, b = 1.37 nm, and γ = 98.3°. (b) Proposed supramolecular structure for the honeycomb A structure of C4-NDI obtained by MD/MM calculation. The calculated unit cell parameters are a = 4.35 nm, b = 4.28 nm, and γ = 119.4°. Corresponding molecules for the bright spots circled in the STM image of panel c are indicated by small red circles in panel d, and the large dark part in the STM is shown as large blue circles in the molecular model. In the model, the structure consists of hexamers (shown as black hexagons) and dimers connecting these hexamers. (c) Honeycomb B structure of C6-NDI obtained by MD/MM calculation. The cell parameters are a = 2.00 nm, b = 2.01 nm, and γ = 119.6°. (d) Model of one unit of the trimer structure of C6-NDI, top and side view. The model structure was obtained by optimization by MOPAC2009 PM6. (e) Structure of C18-NDI obtained by MD/MM calculation. The cell parameters are a = 3.51 nm, b = 0.90 nm, and γ = 95.5°. (f) Another structure for C18-NDI obtained by MD/MM calculation. The cell parameters are a = 3.31 nm, b = 0.91 nm, and γ = 99.2°.

A similar search of **C18-NDI** resulted in a variety of structures because of the flexibility of the long alkyl chain. Two representative structures are shown in Figure 5e,f. In both structures, the NDI cores are aligned along the *b* axis in a manner similar to that in **C3-NDI**. The lengths of the *b* axes are also similar. The difference lies in the arrangement of the alkyl chains. In structure (e), the alkyl chains belonging to a single column of NDI cores are closely packed by themselves, whereas in structure (f), the alkyl chains belonging to two different columns of NDI cores are interpenetrating. The minimized potential energies were too close to determine which structure was preferable.

Honeycomb A Structure. The honeycomb A structure was observed for **C4-NDI** and **C5-NDI**. The observed cell parameters (a = 4.32 nm, b = 4.41 nm, γ = 124°, A = 15.9 nm^2) suggest that Z = 12 (15.9/1.24 = 12.8). Given the apparent six-fold symmetry and the cell parameters, we assumed a hexagonal unit cell having p6 (#16) symmetry. This plane group has six equivalent positions; hence, Z = 12 implies that two independent NDI molecules are contained in the unit cell. The MD simulations that were performed after the geometry search generated several different structures with similar potential energies, and one of them is shown in Figure 5b. This structure is stable during MD calculations at room temperature, has cell parameters (a = 4.28 nm, b = 4.35 nm, γ = 119.4°) similar to the observed values, and corresponds very well with the high-resolution STM image of **C4-NDI**.

Honeycomb B Structure. The honeycomb B structure was observed for the **C6-** to **C9-NDIs**. Regardless of the lengths of the alkyl groups, the observed cell parameters were very similar (a = 1.9−2.0 nm, b = 2.0−2.2 nm, γ = 119−128°, A = 3.34−3.59 nm^2). These results suggest that the structure is mainly determined by the interaction between the NDI cores, rather than the interaction involving the alkyl groups. As we mentioned earlier, we can calculate the maximum number of **C*x*-NDI** molecules contained in this unit cell: that is, 3.5/1.24 = 2.8. This suggests Z = 2 or 3. Because of the apparent six-fold symmetry and cell parameters consistent with a hexagonal unit cell, we first performed the geometry search for Z = 3 in a hexagonal unit cell having p3 (#13) symmetry.[25,26] The geometry of the NDI cores was first determined for **C2-NDI**, and then, the alkyl groups were appended and the system was allowed to fluctuate by MD at room temperature. The calculation for **C6-NDI** ended up with a single, unique structure (Figure 5c). The calculated cell parameters (a = 2.00 nm, b = 2.01 nm, γ = 119.7°) correspond very well with the observed values, and the positions of the NDI cores also correspond well with the bright points in the high-resolution STM image obtained for **C9-NDI**. On the other hand, the geometry search with Z = 2 in an oblique unit cell resulted in various geometries, and some of them were also consistent with the observed honeycomb structure. However, these geometries were unstable during MD calculation at room temperature, resulting in a loss of the characteristic honeycomb structure. Therefore, we conclude that the most likely representation for the honeycomb B structure is that shown in Figure 5c.

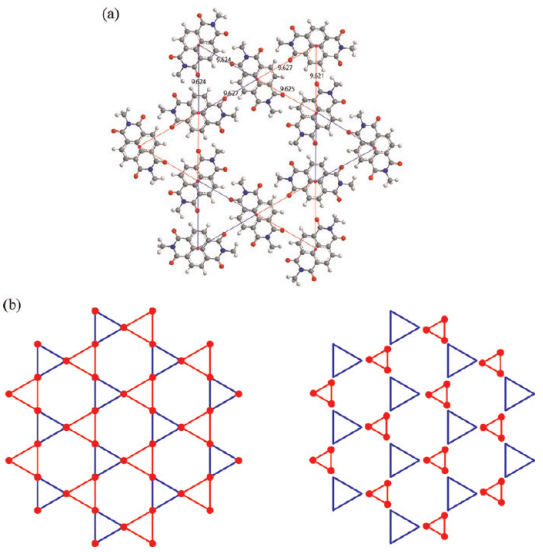

Figure 6. (a) Supramolecular structure of honeycomb B optimized by MOPAC2009 PM6. A small pink circle indicates the centroid of each molecule. (b) Kagome structure made by connecting the centroids of the NDI molecules in the honeycomb B supramolecular structure. A small red circle denotes the centroid of each molecule. If all distances are equal, hexagonal structures appear clearly, as shown in the left figure. In contrast, if the distances between the neighboring molecules in one unit trimer (red triangles in the right figure) are shorter than those in another set of triangles (blue triangles in the right figure), rhombic structure becomes conspicuous because closely packed triangles appear brighter in the STM/AFM images than sparse triangles.

The apparent image of **C9-NDI** observed by FM-AFM (Figure 2k) is different from that observed by STM (Figure 2j). However, we consider that these two supramolecular structures are essentially the same. Figure 6a shows the honeycomb B supramolecular structure obtained by an optimization of **C1-NDI** molecules by MOPAC2009 PM6. By connecting the centroids of the neighboring molecules, a Kagome lattice[27−32] can be formed, as shown in Figure 6b. The structure is made from unit triangles, each consisting of three NDI molecules. In the calculation, the distances between each centroid are almost the same (∼9.62 Å). In such cases, a Kagome lattice is evident, as shown in Figure 2i (**C8-NDI**), in which each triangle's image can be seen clearly by STM. In contrast, when the component molecules in one unit of the triangle molecular system (the red triangles in Figure 6b right) interact more strongly with each other than in the other possible unit triangles (the blue triangles in Figure 6b right), more closely packed triangles are formed by the stronger interaction (the small red triangles), which appear as

brighter spots in STM or AFM images, producing rhombic images resembling those shown in Figure 2k (AFM image of **C9-NDI**). In the STM images of the **C7-** and **C9-NDIs**, three alternate vertices in each hexagonal image show brighter spots than the other three vertices, which can be accounted for by the same reasoning. This indicates that small differences in distance within the Kagome structure cause large variances in the apparent STM and AFM images. The variation in the distances within the Kagome lattice is probably caused by the balance of the interactions between each molecule, between the molecules and the solvent, and between the molecules and the HOPG surface.

Similar honeycomb images are reported for perylenetetracarboxylic dianhydride (PTCDA) on a Ag−Si(111)$\sqrt{3} \times \sqrt{3}R30°$ surface, whose supramolecular structure is assigned to a relaxed form of the combination of a square and a herringbone structure.[33] In the proposed supramolecular structure, there are four independent molecules, forming a hexagonal unit and a centered molecule. For reasons that are unclear, one of the four molecules shows low contrast in the STM measurements, exhibiting an apparent Kagome-lattice-like image. This supramolecular structure is possible for PTCDA because it can form C═O···H−C (aromatic) interactions to stabilize the system. However, the NDIs' *N*-alkyl groups prevent them from forming such a supramolecular structure, which is confirmed by a molecular simulation using molecular orbital (MO) calculations.

Consequently, the Kagome lattice supramolecular structure is the most reasonable structure for the honeycomb B images, given the previously proposed structures for similar molecules,[21,23] and other honeycomb images can be tentatively assigned to modified Kagome structures (some of them are depicted in the Supporting Information).

Discussion on the Variation in Supramolecular Structures with the NDI Alkyl Chain Length. On the basis of MD/MM calculations, the supramolecular structures can be assigned to two categories: lamellar and honeycomb structures. The areas that single molecules occupy on the surface, calculated from STM measurements, are plotted against alkyl chain length in Figure 3. As discussed earlier, the areas of the honeycomb A, B, and C structures are independent of the lengths of the chains, while lamellar structures generally depend on the chain length. For lamellar structures, the area of a single molecule can be fitted as follows: area(lamellar) = 1.4 + 0.1*N* nm^2, where *N* denotes the chain length. The area estimated from the Connolly solvent-excluded volume, and the typical thickness of the π-conjugated plane (0.38 nm) is described by area(Connolly) = 0.51 + 0.10*N*.[34] The calculated area corresponding to one methylene unit is consistent with the observed value, while the observed value (1.4 nm^2) of the imide core is larger than the calculated one (0.51 nm^2). This implies that the lamellar structures observed on the graphite surface are looser than those of the close-packed structure. The most important finding is that the areas observed for honeycomb structures are smaller than those estimated from the Connolly volume, as indicated in Figure 3 by a solid line. This reasonably shows that the alkyl chains do not lie on the surface in the honeycomb structures, as already discussed in the previous section. The proposed structure of typical honeycomb formations is shown in Figure 5c, which depicts the trimer structures shown in Figure 5d, in which all of the alkyl chains are standing up from the surface.

A question arises as to why only the **C4-** to **C12-NDIs** adopt supramolecular structures with the alkyl chains standing on the surface, and why the **C3-**, **C4-**, and **C14-** to **C18-NDIs** show lamellar structures with the alkyl chains lying on the surface. There are four main possible driving forces for determining the supramolecular structures of NDI derivatives on graphite: (i) alkyl−graphite interaction (molecular−substrate interaction); (ii) NDI core and graphite interaction (molecular−substrate interaction); (iii) van der Waals interactions between alkyl chains (intermolecular interaction); (iv) CH−O interaction between NDI molecules (intermolecular interaction). As the alkyl chain length is increased, both (i) the alkyl−graphite interaction and (iii) the van der Waals interactions between alkyl chains increase, while (ii) the NDI core and graphite interaction remains unchanged. The main difference in the energy between the lamellar structures and the honeycomb structures originates in the interactions of alkyl chains with the graphite surface or those of the alkyl chains with each other. If the interaction energy of the former is favored, the lamellar structures should be more stable for any chain length of NDI; if the situation is the opposite, all of the structures should be honeycomb structures. This implies that the consideration of only the energies cannot account for the dependence of the observed supramolecular structures on the chain length.

Next, we consider the entropy term of each supramolecular structure and see how it affects the dependence of the structures on the chain length. Thermodynamic entropy, *S*, can be expressed as $S = k_B \ln(\Omega)$, where k_B is the Boltzmann constant and Ω denotes the number of cases. In the simplest approximation for nonbranching polymers, $\Omega = Z^N$, where *Z* is the number of possible conformations per each monomer unit and *N* is the chain length. In polymer science, the value $Z = 6$ is usually used for discussions within the lattice model because the number of the nearest neighbors of the lattice is 6,[35] whereas in the case of alkyl chains, $Z = 3$ would be more appropriate. In either case, the entropy is $S(N) = -k_B N \log(Z)$, which is proportional to the length of the chain (*N*). Because the enthalpy term

(H) related to the alkyl chain is linearly proportional to N, the Gibbs free energy ($G = H - TS$) is also linearly dependent on N. With this simplest model, the expected change of the supramolecular structures should be only in one direction (lamellar to honeycomb or *vice versa*). However, this is in contrast with the observed behavior, where the structure changes from lamellar to honeycomb and then back again to lamellar. In order to account for this complex behavior, a nonlinear term should be introduced into the thermodynamic parameters depending on the chain length. In the following, we will discuss this point, first in a general manner and then in a specific manner.

More realistic treatment of entropy of nonbranching polymers includes the effect of the excluded volume, which causes decrease of Ω by self-intersections, leaving only "self-avoiding walks". It is not simple to calculate the number of self-avoiding walks, and many trials have been reported on it.[36−39] Fortunately, for shorter chain lengths ($5 \leq N \leq 20$), the results of a direct counting method are available, which can be analytically fitted with the equation $S(N) = -k_B(1.5N + 0.18\log(N) - 1.4)$.[40] For $N \rightarrow \infty$, $S(N)/(-k_BN) = 1.5$, whereas for shorter chains, $S(N)/(-k_BN)$ is less than 1.5. This implies that, for longer alkyl chains, the entropy lost by straightening the relaxed (and bent) chain is linearly proportional to the chain length; however, for shorter chains, the loss of entropy is smaller than the value estimated by the linearity. Let us consider the change in the Gibbs free energy $\Delta G_{H\rightarrow L}(N)$ for the transformation of honeycomb structures to lamellar structures. We can reasonably estimate that, by this transformation, the $\Delta H_{H\rightarrow L}(N)$ term is negative (favored) because the interactions of the alkyl chains with the graphite surface produce a gain in energy, and the ΔS term is unfavored (that is, negative) because, in the lamellar structures, the alkyl chains are straight, and the entropy should be less than that for honeycomb structures where the alkyl chains are randomly movable within the solution. In order to analyze this in a semiquantitative manner, the following values are defined: ΔH_0, enthalpy change that does not depend on the chain length; ΔS_0, entropy change that does not depend on the chain length; ΔH_1, enthalpy change for one methylene unit; $\Delta S_{H\rightarrow L}(N)$, entropy change dependent on chain length. Since the Ω relevant to the methylene groups for the lamellar structures is nearly 1, or very near to the minimum, we can deduce the following equation: $\Delta S_{H\rightarrow L}(N) = -k_B(1.5N + 0.18\log(N) - 1.4)$. So, the change in Gibbs free energy for the transformation of honeycomb structures to lamellar structures can be expressed as follows:

$$\Delta G_{H\rightarrow L}(N) = (\Delta H_0 - T\Delta S_0) + N\Delta H_1 + k_BT(1.5N + 0.18\log(N) - 1.4)$$

This function depending on N is convex upward, and thus it is possible that the value is positive only in a limited range of N and is negative outside the range. Such a behavior is consistent with the observation that honeycomb structures are only formed in the range $4 \leq N \leq 12$; for $N = 3$, 4, and $N > 12$, lamellar structures are favored ($\Delta G_{H\rightarrow L}(N) < 0$).

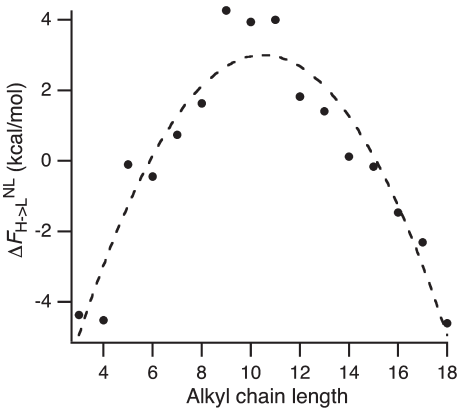

Figure 7. Nonlinear component of the calculated free energy from the honeycomb to the lamellar structures.

The above discussion only deals with general characteristics of alkyl chains. To include specific structural details of the ***Cn*-NDI**/HOPG system, we utilized molecular dynamics (MD) calculations. The free energy of a certain structure can be estimated by free energy perturbation calculations.[41] The calculation details are described in the Methods section. Because of the limitation of the computational resources, our calculations ignore many important interactions, most notably the solvent effects. Although this will lead to significant bias in the estimated free energy, we can expect the bias will be linear on N because it is mostly related to the enthalpic contribution. Therefore, we will focus on the "nonlinear" component of the calculated free energy. The calculated $\Delta F_{H\rightarrow L}(N)$ (the change in Helmholtz free energy for the transformation of honeycomb structures to lamellar structures) was convex upward, which is consistent with the general discussion described above. After subtracting the linear component by regression analysis, the nonlinear component of $\Delta F_{H\rightarrow L}(N)$, $\Delta F_{H\rightarrow L}{}^{NL}(N)$, was estimated as shown in Figure 7. The nonlinear component has a maximum at $N = 9-11$, which is roughly consistent with the observation that the honeycomb structure is preferred for $4 \leq N \leq 12$.

A subtle interplay of packing and entropic effects on two-dimensional supramolecular structures has been proposed for alkane chains physisorbed on graphite.[42] One STM study suggests that the zigzag planes are oriented perpendicular to the graphite surface.[16] The authors have obtained molecular adsorption energies by MD calculations to show that the conformation with zigzag planes oriented parallel to the graphite is energetically favored over that where they are oriented perpendicular; however, the energetically favored conformation is not necessarily thermally

stable. In prolonged MD calculations, the energetically unfavored structure (with the zigzag plane oriented perpendicular to the graphite surface) becomes dominant. The authors suggest that this results from the entropy effect. Aside from the pioneering work of these authors, there are very few papers that describe the importance of the entropy term to the determination of supramolecular structures on a surface.

CONCLUSION

Although several papers have reported the dependence of two-dimensional supramolecular structures on alkyl chain length,[6,9,11] such a drastic change in structure, as observed in the present work for NDIs, is rare. The supramolecular structure for each STM or FM-AFM image is assigned with the help of molecular simulations, showing that the **C3-** and **C4-NDIs** have lamellar structures, that the **C4-** to **C12-NDIs** show honeycomb structures or modifications thereof, and that NDIs with longer alkyl chains than C12 exhibit lamellar structures again. The drastic change from lamellar to honeycomb (Kagome lattice) and then back to lamellar depending on the chain length can be explained by the balance of entropy and enthalpy terms. In the honeycomb structures, the alkyl chains stand up from the surface, which is unfavored in enthalpy terms (ΔH) but favored in entropy terms (ΔS). The dependence of the entropy term on the chain length is not linear because of the "self-avoiding" in relatively short chain lengths, which reasonably accounts for the complex change in the supramolecular structure.

Here we were able to clearly show the importance of the entropy term in the control of two-dimensional supramolecular structures on a surface, and we believe that this will provide a clue for predicting and describing supramolecular structures using their unit molecular structures.

Generality of our discussion will be the challenging future target. There can be many possible factors which can affect the supramolecular structures on a surface: the concentration of the solution, the solvent properties, surface substrate, and the molecular structures. Since the supramolecular structure formation is mainly governed by equilibrium, the concentration of the sample will not affect sharply the patterns formed on the surface. The solvent properties and surface substrate will change the balance of the parts of the molecules to stay on the surface or within the solution. If you use solvents which favor alkyl chains, the range of the alkyl chain length which shows the honeycomb structures can be broadened. Influence of the molecular structures will be the most challenging part to be clarified.

METHODS

Materials and Organic Synthesis. 1-Tetradecene was purchased from Nacalai Tesque and purified by silica gel chromatography for use as the solvent. Other solvents and reagents were purchased from Aldrich, Kanto, or TCI and used as received. ^{1}H NMR spectra were recorded with a JEOL JNM-LA400 spectrometer, with $CDCl_3$ as the solvent. Chemical shifts (δ) were calibrated by using tetramethylsilane (TMS), and the residual solvent peak was set as the internal standard. Fourier transform infrared (FT-IR) spectra were obtained from KBr pellets with a JASCO FT/IR-460 plus. Mass spectra (MS) were obtained using an Applied Biosystems Voyager DE-STR with no matrix. Column chromatography was carried out with a Yamazen preparative chromatography system, YFLC-5404-FC-GRII, and a Hi-Flash column.

General Syntheses of Naphthalenediimide Derivatives. *N*,*N*′-Bis(*n*-butyl)naphthalenediimide (**C4-NDI**), *N*,*N*′-bis(*n*-nonyl)naphthalenediimide (**C9-NDI**), and *N*,*N*′-bis(*n*-octadecyl)naphthalenediimide (**C18-NDI**) derivatives were prepared according to the previously reported procedure.[43] Other derivatives were prepared by a modified procedure. Full compound data are available in the Supporting Information.

STM Measurement. HOPG was obtained from Veeco instruments. STM tips were mechanically formed from Pt/Ir (70/30) wire (0.2 mm in diameter). The STM observation was performed using a JEOL JSPM-5200, with a handmade liquid cell for the solid−liquid interface measurements.

The compound was dissolved in 1-tetradecene ($\sim$5.0 $\times$ 10^{-4} M) at 100 °C. Drops of solution were deposited onto the freshly cleaved HOPG surfaces fixed in the handmade cell. The substrate was kept at 100 °C for 5 min and cooled to room temperature. Without the annealing, stable supramolecular structures cannot be observed. The STM tip was immersed in the solution to record images at the solid−liquid interface, in the constant current mode and at room temperature. The lattice parameters were determined using several STM images and calibrated using the HOPG lattice ($a = b = 0.246$ nm, $\gamma = 120°$) as a reference.[44] The STM images of graphite for the lattice parameter calibration were obtained by decreasing the bias voltage in the same area where the STM images for the molecular lattice parameters were obtained. STM images were processed by low-pass filtering and line averaging. The resolutions of the STM images are generally dependent on the stability of the molecular film made on the HOPG surface, STM tip conditions, and the conditions of the STM machine. The images shown in Figure 2 have different scaling because we like to depict the best resolution images as possible.

FM-AFM Measurements. FM-AFM experiments were performed in liquids using a commercially available AFM (Shimadzu SPM-9600) modified with a low-noise optical beam deflection sensor. The deflection noise was less than 20 fm/Hz. We used gold-coated, highly doped silicon cantilevers (Nanosensors PPP-NCHAuD) with a resonance frequency of about 160 kHz, a spring constant of about 40 N/m, and a *Q*-factor of around 10 in water, as force sensors. All measurements were carried out at room temperature. The topography was observed in the constant frequency shift mode, where the frequency shift of the cantilever resonance frequency induced by the tip−sample interaction was kept constant for a given tip−sample distance. The cantilever was vibrated in the constant amplitude mode, where the cantilever oscillation amplitude was kept constant by adjusting the amplitude of a cantilever excitation signal. The amplitude was set to 6 nm in imaging scans. The solution droplets of the samples were placed onto a freshly cleaved HOPG substrate. After drying the surface, the sample was placed in a liquid cell and immersed in pure water. FM-AFM images were taken in pure water; for the same solvent as that used during the STM measurement, no clear image could be obtained.

Molecular Modeling Calculations of NDI Derivatives. Molecular modeling calculations were performed on the basis of interatomic potentials used in molecular mechanics. The force field parameters were taken from the parm99 and gaff parameter sets distributed with AMBER 7.[45] The calculations were carried

out with the NAMD program package[46] and homemade programs. The electrostatic interactions were modeled by the restrained electrostatic potential fit (RESP) method.[47] The RESP charges for individual atoms were obtained by a quantum mechanical calculation of the electrostatic potential (HF/6-31G*) with GAMESS (US),[48] followed by fitting with the RESP program module of AMBER. This calculation was done for **C1-NDI** (*N*,*N*′-dimethyl-1,4,5,8-naphthalenetetracarboxylic diimide). For other compounds with longer alkyl groups, the RESP charges of the C/H atoms in the alkyl chain were set to zero (except for the CH_2 group directly attached to the imide N, for which the RESP charges for **C1-NDI** were used). The nonbonding interactions were cut off at 0.9 nm. The electrostatic interactions were modified according to the XPLOR-style shift function, as implemented in NAMD, whereas the van der Waals interactions were simply offset by the calculated value at the cutoff distance.

The technical details of the computation will be reported in a separate paper, and they are only briefly described here. The HOPG surface was modeled as an infinite array of regular hexagons of carbon atoms (type "CA" in the parm99 notation) with a shortest C−C distance of 0.123 nm. This surface was placed on the *xy* plane. In order to account for the regular packing of **C*x*-NDI** molecules, two-dimensional periodic boundary conditions were assumed. This caused a subtle conflict with the HOPG model because the lattice constants of the adsorbed molecules would not necessarily coincide with the multiples of the lattice constants of the HOPG surface. To work around this conflict, the potentials of **C*x*-NDI**/HOPG interactions were averaged over 25 unit cells of **C*x*-NDI** (5 units along each of the two axes).

To find suitable models for the STM results, a set of random orientations of **C*x*-NDI** were generated to match the observed symmetry and lattice parameters, and the models with reasonable energies were selected using a genetic algorithm.[49] After several candidate structures were obtained, they were subjected to molecular dynamics (MD) simulations at 300 K to allow thermal fluctuation. The structures with the lowest potential energies were taken from the MD trajectory, and the potential energies were minimized to yield the final models. The MD conditions were as follows: the time step was 1 fs; the total simulation time was 1 ns; the temperature was kept at 300 K by the use of an Andersen thermostat.[50] The unit cell parameters of the periodic boundary conditions were allowed to fluctuate under constant external pressure (1.0 bar).[51] The visualization of the resulting structures and MD trajectories were executed using VMD.[52] Calculations were performed on a local cluster of Apple PowerMac G5 machines.

Free Energy Perturbation Calculations. The entropy of the honeycomb structure was estimated by the free energy perturbation method.[41]

Since we are only interested in the dependence of the entropy on the alkyl chain length, we fix the NDI core as in the honeycomb B structure of **C6-NDI**. To each of the three NDI molecules within the unit cell, a CH_3 group was attached (**C1-NDI**). Starting from this structure, free energy perturbation was performed so that one of the hydrogen atoms of each CH_3 group was gradually converted to a CH_3 group (to form **C2-NDI**). During the transformation, the NDI core atoms were fixed, and the nonbonding interactions involving the vanishing and appearing atoms were scaled by $(1 - \lambda)$ and λ, respectively, where λ is the transformation parameter ($\lambda = 0$ and 1 represent **C1-NDI** and **C2-NDI**, respectively). Integration of the quantity $-RT \ln \langle \exp(-\delta U/RT) \rangle_\lambda$ ($\langle ... \rangle_\lambda$ denotes an ensemble average with given λ and δU is the change of potential energy between λ and $\lambda + \delta\lambda$) over $\lambda = 0$ to 1 gives the (Helmholtz) free energy change $\Delta F_{1\to2}$ for this transformation. On the other hand, change of the internal energy is given by the ensemble average of the internal energy: $\Delta U_{1\to2} = \langle U \rangle_\lambda$. To derive the entropy of formation of the honeycomb structure for the particular alkyl length, we needed to perform another hypothetical transformation, in which all nonbonding interactions involving the vanishing and appearing atoms were ignored (*i.e.*, even self-crossing of the alkyl chains was allowed for longer chains). The destination state of this transformation has "free" alkyl groups without any nonbonding interaction and can be used as the reference state for the entropy calculation. Let $\Delta F'_{1\to2}$ and $\Delta U'_{1\to2}$ denote the free energy and the internal energy change for this transformation. We can assume $\Delta F'_{1\to2} = 0$ because δU is always zero. Thus, the entropy of the honeycomb **C2-NDI** structure in reference to the "free" alkyl state can be calculated by the following equation.

$$\Delta S_2 = (\Delta U_2 - \Delta F_2)/T = ((\Delta U_{1\to2} - \Delta U'_{1\to2}) - \Delta F_{1\to2})/T$$

The entropies of the honeycomb structures of **C*n*-NDI** ($n \geq 3$) were calculated in a similar way, by transforming one of the terminal hydrogen atoms in **C(*n*−1)-NDI** to a methyl group. On the other hand, the entropies of the lamellar structures of **C*n*-NDI** were assumed to be $R(n-1)\log 3$ because the "free" alkyl chains have 3^{n-1} possible conformations of the methylene groups, whereas the lamellar structures have a single restricted conformation (or only a small number of conformations), so that $\Delta S_{2,\text{lamellar}} = R \log 3^{n-1} - R \log 1 = R(n-1)\log 3$.

Conflict of Interest: The authors declare no competing financial interest.

Acknowledgment. This work was funded by a grant-in-aid for scientific research on innovative areas (No. 20111012). Studies using FM-AFM were supported by the SENTAN program of the Japan Science and Technology Agency (JST).

Supporting Information Available: (1) Analytical and spectral characterization of the NDIs. (2) Supramolecular structure assignment of the Honeycomb images. (3) Eye guidance to help analysis of the STM images. This material is available free of charge *via* the Internet at http://pubs.acs.org.

REFERENCES AND NOTES

1. Plass, K. E.; Grzesiak, A. L.; Matzger, A. J. Molecular Packing and Symmetry of Two-Dimensional Crystals. *Acc. Chem. Res.* **2007**, *40*, 287–293.
2. Elemans, J.; De Cat, I.; Xu, H.; De Feyter, S. Two-Dimensional Chirality at Liquid−Solid Interfaces. *Chem. Soc. Rev.* **2009**, *38*, 722–736.
3. Otsuki, J. STM Studies on Porphyrins. *Coord. Chem. Rev.* **2010**, *254*, 2311–2341.
4. Haq, S.; Liu, N.; Humblot, V.; Jansen, A. P. J; Raval, R. Drastic Symmetry Breaking in Supramolecular Organization of Enantiomerically Unbalanced Monolayers at Surfaces. *Nat. Chem.* **2009**, *1*, 409–414.
5. Tao, F.; Bernasek, S. L. Understanding Odd-Even Effects in Organic Self-Assembled Monolayers. *Chem. Rev.* **2007**, *107*, 1408–1453.
6. Phillips, T. K.; Bhinde, T.; Clarke, S. M.; Lee, S. Y.; Mali, K. S.; Freyter, S. D. Adsorption of Aldehyde on a Graphite Substrate: Combined Thermodynamic Study of C6−C13 Homologues with Structural and Dynamical Study of Dodecanal. *J. Phys. Chem. C* **2010**, *114*, 6027–6034.
7. Zhang, X.; Chen, T.; Chen, Q.; Deng, G. J.; Fan, Q. H.; Wan, L. J. One Solvent Induces a Series of Structural Transitions in Monodendron Molecular Self-Assembly from Lamellar to Quadrangular to Hexagonal. *Chem.—Eur. J.* **2009**, *15*, 9669–9673.
8. Zhang, X.; Chen, Q.; Deng, G.-J.; Fan, Q.-H.; Wan, L.-J. Structural Diversity of a Monodendron Molecule Self-Assembly in Different Solvents Investigated by Scanning Tunneling Microscopy: From Dispersant to Counterpart. *J. Phys. Chem. C* **2009**, *113*, 16193–16198.
9. Kikkawa, Y.; Koyama, E.; Tsuzuki, S.; Fujiwara, K.; Kanesato, M. Bipyridine Derivatives at a Solid/Liquid Interface: Effects of the Number and Length of Peripheral Alkyl Chains. *Langmuir* **2010**, *26*, 3376–3381.
10. Kikkawa, Y.; Kihara, H.; Takahashi, M.; Kanesato, M.; Balaban, T. S.; Lehn, J. M. Two-Dimensional Structures of Anthracene Derivatives: Photodimerization and Host−Guest Chemistry. *J. Phys. Chem. B* **2010**, *114*, 16718–16722.
11. Florio, G. M.; Werblowsky, T. L.; Ilan, B.; Muller, T.; Berne, B. J.; Flynn, G. W. Chain-Length Effects on the Self-Assembly of Short 1-Bromoalkane and *n*-Alkane Monolayers on Graphite. *J. Phys. Chem. C* **2008**, *112*, 18067–18075.
12. Ilan, B.; Florio, G. M.; Hybertsen, M. S.; Berne, B. J.; Flynn, G. W. Scanning Tunneling Microscopy Images of Alkane Derivatives on Graphite: Role of Electronic Effects. *Nano Lett.* **2008**, *8*, 3160–3165.

13. Zhang, X.; Yan, C.-J.; Pan, G.-B.; Zhang, R.-Q.; Wan, L.-J. Effect of C−H···F and O−H···H Hydrogen Bonding in Forming Self-Assembled Monolayers of BF2-Substituted β-Dicarbonyl Derivatives on HOPG: STM Investigation. *J. Phys. Chem. C* **2007**, *111*, 13851–13854.
14. Rohde, D.; Yan, C.-J.; Yan, H.-J.; Wan, L.-J. From a Lamellar to Hexagonal Self-Assembly of Bis(4,4′-(*m*,*m*′-di(dodecyloxy-)phenyl)-2,2′-difluoro-1,3,2-dioxaborin) Molecules: A Trans-to-Cis-Isomerization-Induced Structural Transition Studied with STM. *Angew. Chem., Int. Ed.* **2006**, *45*, 3996–4000.
15. Thalacker, C.; Miura, A.; Feyter, S. D.; Schryver, F. C. D.; Wurthner, F. Hydrogen Bond Directed Self-Assembly of Core-Substituted Naphthalene Bisimides with Melamines in Solution and at the Graphite Interface. *Org. Biomol. Chem.* **2005**, *3*, 414–422.
16. Rabe, J. P.; Buchholz, S. Commensurability and Mobility in Two-Dimensional Molecular Patterns on Graphite. *Science* **1991**, *253*, 424–427.
17. Elemans, J.; Lei, S. B.; De Feyter, S. Molecular and Supramolecular Networks on Surfaces: From Two-Dimensional Crystal Engineering to Reactivity. *Angew. Chem., Int. Ed.* **2009**, *48*, 7298–7332.
18. Fukuma, T.; Kimura, M.; Kobayashi, K.; Matsushige, K.; Yamada, H. Development of Low Noise Cantilever Deflection Sensor for Multienvironment Frequency-Modulation Atomic Force Microscopy. *Rev. Sci. Instrum.* **2005**, *76*, 053704.
19. Rode, S.; Oyabu, N.; Kobayashi, K.; Yamada, H.; Kuhnle, A. True Atomic-Resolution Imaging of (1014) Calcite in Aqueous Solution by Frequency Modulation Atomic Force Microscopy. *Langmuir* **2009**, *25*, 2850–2853.
20. Hiasa, T.; Kimura, K.; Onishi, H.; Ohta, M.; Watanabe, K.; Kokawa, R.; Oyabu, N.; Kobayashi, K.; Yamada, H. Solution-TiO_2 Interface Probed by Frequency-Modulation Atomic Force Microscopy. *Jpn. J. Appl. Phys.* **2009**, *48*, 08JB19.
21. Kaneda, Y.; Stawasz, M. E.; Sampson, D. L.; Parkinson, B. A. STM Investigations of the Two-Dimensional Ordering of Perylenetetracarboxylic Acid *N*-Alkyl-Diimides on HOPG and MoS_2 Surfaces. *Langmuir* **2001**, *17*, 6185–6195.
22. Kendrick, C.; Kahn, A.; Forrest, S. R. STM Study of the Organic Semiconductor PTCDA on Highly-Oriented Pyrolytic Graphite. *Appl. Surf. Sci.* **1996**, *104/105*, 586–594.
23. Kleiner-Shuhler, L.; Brittain, R.; Johnston, M. R.; Hipps, K. W. Scanning Tunneling Microscopy and Orbital-Mediated Tunneling Spectroscopy of *N*,*N*′-Dioctyl-1,8:4,5-naphthalenediimide Adsorbed on Highly Ordered Pyrolytic Graphite from Various Solvents and in Different Environments. *J. Phys. Chem. C* **2008**, *112*, 14907–14912.
24. Alvey, P.; Reczek, J.; Lynch, V.; Iverson, B. A Systematic Study of Thermochromic Aromatic Donor−Acceptor Materials. *J. Org. Chem.* **2010**, *75*, 7682–7690.
25. *International Tables for Crystallography: Space-Group Symmetry*, 5th ed.; Springer: Berlin, 2005; Vol. A.
26. Since the six-fold symmetry was observed, it would have been more consistent to assume the p6 (#16) plane group. In this case, we would have needed to place one NDI molecule on the special position having the *C*2 symmetry (*e.g.*, (0.5, 0.5)) to conform with the assumption of $Z = 3$. However, it was not necessary for us to assume this higher symmetry because the calculation with the p3 symmetry eventually gave the same result.
27. Mao, J.; Zhang, H.; Jiang, Y.; Pan, Y.; Gao, M.; Xiao, W.; Gao, H.-J. Tunability of Supramolecular Kagome Lattices of Magnetic Phthalocyanines Using Graphene-Based Moire Pattern as Templates. *J. Am. Chem. Soc.* **2009**, *131*, 14136–14137.
28. Schlickum, U.; Decker, R.; Klappenberger, F.; Zoppellaro, G.; Klyatskaya, S.; Auwarter, W.; Neppl, S.; Kern, K.; Brune, H.; Ruben, M.; *et al.* Chiral Kagome Lattice from Simple Ditopic Molecular Bricks. *J. Am. Chem. Soc.* **2008**, *130*, 11778–11782.
29. Tahara, K.; Furukawa, S.; Uji-I, H.; Uchino, T.; Ichikawa, T.; Zhang, J.; Mamdouh, W.; Sonoda, M.; De Schryver, F. C.; De Feyter, S.; *et al.* Two-Dimensional Porous Molecular Networks of Dehydrobenzo[12]Annulene Derivatives *via* Alkyl Chain Interdigitation. *J. Am. Chem. Soc.* **2006**, *128*, 16613–16625.
30. Tahara, K.; Okuhata, S.; Adisoejoso, J.; Lei, S. B.; Fujita, T.; De Feyter, S.; Tobe, Y. 2D Networks of Rhombic-Shaped Fused Dehydrobenzo[12]Annulenes: Structural Variations under Concentration Control. *J. Am. Chem. Soc.* **2009**, *131*, 17583–17590.
31. Tahara, K.; Lei, S. B.; Adisoejoso, J.; De Feyter, S.; Tobe, Y. Supramolecular Surface-Confined Architectures Created by Self-Assembly of Triangular Phenylene-Ethynylene Macrocycles *via* van der Waals Interaction. *Chem. Commun.* **2010**, *46*, 8507–8525.
32. Shi, Z.; Lin, N. Porphyrin-Based Two-Dimensional Coodination Kagome Lattice Self-Assembled on a Au(111) Surface. *J. Am. Chem. Soc.* **2009**, *131*, 5376–5377.
33. Swarbrick, J. C.; Ma, J.; Theobald, J. A.; Oxtoby, N. S.; O'Shea, J. N.; Champness, N. R.; Beton, P. H. Square, Hexagonal and Row Phases of PTCDA and PTCDI on Ag-Si(111)$\sqrt{3}\times\sqrt{3}R30°$. *J. Phys. Chem. B* **2005**, *109*, 12167–12174.
34. Connolly, M. L. Computation of Molecular Volume. *J. Am. Chem. Soc.* **1985**, *107*, 1118–1124.
35. Vorontsov-Velyaminov, P. N.; Volkov, N. A.; Yurchenko, A. A. Entropic Sampling of Simple Polymer Models within Wang−Landau Algorithm. *J. Phys. A* **2004**, *37*, 1573–1588.
36. Duda, J.; Milewskaduda, J. A Theoretical-Model for Evaluation of Configurational Entropy of Mixing with Respect to Shape and Size of Particles. *J. Math. Chem.* **1995**, *17*, 69–109.
37. Douglas, J.; Guttman, C. M.; Mah, A.; Ishinabe, T. Spectrum of Self-Avoiding Walk Exponents. *Phys. Rev. E* **1997**, *55*, 738–749.
38. Nakamura, I.; Shi, A. C. Study of Entropy-Driven Self-Assembly of Rigid Macromolecules. *Phys. Rev. E* **2009**, *80*, 021112.
39. White, R. P.; Funt, J.; Meirovich, H. Calculation of the Entropy of Lattice Polymer Models from Monte Carlo Trajectries. *Chem. Phys. Lett.* **2005**, *410*, 430–435.
40. Zhao, D.; Huang, Y.; He, Z.; Quan, R. Monte Carlo Simulation of the Conformational Entropy of Polymer Chains. *J. Chem. Phys.* **1996**, *104*, 1672–1674.
41. Kollman, P. Free Energy Calculations: Applications to Chemical and Biochemical Phenomena. *Chem. Rev.* **1993**, *93*, 2395–2417.
42. Hentschke, R.; Shchurmann, B. L.; Rabe, J. P. Molecular Dynamics Simulations of Ordered Alkane Chains Physisorbed on Graphite. *J. Chem. Phys.* **1992**, *96*, 6213–6221.
43. Ozser, M. E.; Uzun, D.; Elci, I.; Icil, H.; Demuth, M. Novel Naphthalene Diimides and a Cyclophane Thereof: Synthesis, Characterization, Photophysical and Electrochemical Properties. *Photochem. Photobiol. Sci.* **2003**, *2*, 218–223.
44. Hoshino, A.; Isoda, S.; Kurata, H.; Kobayashi, T. Scanning Tunneling Microscope Contrast of Perylene-3,4,9,10-tetracarboxylic-dianhydride on Graphite and Its Application to the Study of Epitaxy. *J. Appl. Phys.* **1994**, *76*, 4113–4120.
45. Case, D. A.; Pearlman, D. A.; Caldwell, J. W.; Cheatham, E. C., III; Wang, J.; Ross, W. S.; Simmerling, C.; Darden, T.; Merz, K. M.; Stanton, R. V.; *et al. Amber 7*; San Francisco, 2002.
46. Phillips, A. C.; Braun, R.; Wang, W.; Gumbart, J.; Tajkhorshid, E.; Villa, E.; Chipot, C.; Skeel, R. D.; Kale, L.; Schulten, K. *J. Comput. Chem.* **2005**, *26*, 1781–1802.
47. Bayly, C. I.; Cieplak, P.; Cornell, W.; Kollman, P. A. A Well-Behaved Electrostatic Potential Based Method Using Charge Restraints for Deriving Atomic Charges: The Resp Model. *J. Phys. Chem.* **1993**, *97*, 10269–10280.
48. Schmidt, M. W.; Baldridge, K. K.; Boatz, J. A.; Elbert, S. T.; Gordon, M. S.; Jensen, J. H.; Koseki, S.; Matsunaga, N.; Nguyen, K. A.; Su, S. J.; *et al.* General Atomic and Molecular Electronic Structure System. *J. Comput. Chem.* **1993**, *14*, 1347–1363.
49. Nagata, T. Automated Design of Protecting Molecules for Metal Nanoparticles by Combinatorial Molecular Simulations. *J. Organomet. Chem.* **2007**, *692*, 225–233.

50. Andersen, H. C. Molecular Dynamics Simulations at Constant Pressure and/or Temperature. *J. Chem. Phys.* **1980**, *72*, 2384–2393.
51. Lill, J. V.; Broughton, J. Q. Nonlinear Molecular Dynamics and Monte Carlo Algorithms. *Phys. Rev. B* **1992**, *46*, 12068–12071.
52. Humphrey, W.; Dalke, A.; Schulten, K. VMD: Visual Molecular Dynamics. *J. Mol. Graphics* **1996**, *14*, 33–38.